

Polarization of high-energy pulsar radiation in the striped wind model

J. Pétri¹ and J. G. Kirk¹

Max-Planck-Institut für Kernphysik, Saupfercheckweg 1, 69117 Heidelberg, Germany.

Jerome.Petri@mpi-hd.mpg.de

John.Kirk@mpi-hd.mpg.de

ABSTRACT

The Stokes parameters of the pulsed synchrotron radiation produced in the striped pulsar wind model are computed and compared with optical observations of the Crab pulsar. We assume the main contribution to the wind emissivity comes from a thin transition layer where the dominant toroidal magnetic field reverses its polarity. The radial component of the field is neglected, but a small meridional component is added. The resulting radiation is linearly polarized (Stokes $V = 0$). In the off-pulse region, the electric vector lies in the direction of the projection on the sky of the rotation axis of the pulsar. This property is unique to the wind model and in good agreement with the data. Other properties such as a reduced degree of polarization and a characteristic sweep of the polarization angle within the pulses are also reproduced. These properties are qualitatively unaffected by variations of the wind Lorentz factor, the electron injection power law index and the inclination of the line of sight.

Subject headings: MHD — Plasmas — Polarization — Pulsars: general — Radiation mechanisms: non-thermal

1. Introduction

The high-energy, pulsed emission from rotating magnetized neutron stars is usually explained in the framework of either the polar cap (Sturrock 1971; Ruderman & Sutherland 1975) or the outer gap models (Cheng et al. 1986; Hirotani & Shibata 1999), for a review

see (Harding 2001). Although the existence of such gaps is plausible (Pétri et al. 2002), these models still suffer from the lack of a self-consistent solution for the pulsar magnetosphere and are based on the assumption that the magnetic field structure is that of a (Newtonian) rotating dipole. Nevertheless, recent observations of the polarization of the optical pulses from the Crab (Kellner 2002; Kanbach et al. 2003) motivated detailed comparative studies of the emission from these models (Dyks et al. 2004) as well as a new variant of the outer gap introduced by Dyks & Rudak (2003) and called the “two-pole caustic” model. This model has a gap extending from the light-cylinder to the polar caps. It reproduces the twin-peak pulse intensity profiles by associating each peak with a different magnetic pole. In all of these models, the radiation is produced within the light cylinder. However, the pulse profile is determined by the assumed geometry of the magnetic field and the location of the gaps. Despite earlier claims (Romani & Yadigaroglu 1995), it now appears that neither the polar cap nor the outer gap model are able to fit the optical polarization properties of the Crab pulsar. The two-pole caustic model, on the other hand, provides a qualitatively reasonable fit (Dyks et al. 2004).

An alternative site for the production of pulsed radiation has been investigated recently (Kirk et al. 2002), based on the idea of a striped pulsar wind, originally introduced by Coroniti (1990) and Michel (1994) and elaborated by Lyubarsky & Kirk (2001) and Kirk & Skjæraasen (2003). Compared to the inner, outer and slot gaps, much less progress has been made in understanding the particle acceleration problem in this model. As proposed by Lyubarskii (1996), it is assumed that magnetic energy is released by reconnection in the thin regions where the toroidal field reverses its polarity, producing a non thermal electron/positron population. But, unlike in Lyubarsky’s model, emission from the striped wind originates outside the light cylinder and relativistic beaming effects are responsible for the phase coherence of the synchrotron radiation. A strength of this model is that the geometry of the magnetic field, which is the key property determining the polarization properties of the emission, is relatively well-known. Because relativistic, magnetically dominated winds seem to collimate only very weakly (Bogovalov 2001; Vlahakis 2004), the dominant field component well outside the light-cylinder is toroidal, irrespective of the geometry of the magnetic field near the stellar surface.

In this Letter, we use an explicit asymptotic solution for the large-scale field structure related to the oblique split monopole and valid for the case of an ultrarelativistic plasma (Bogovalov 1999). This is combined with a crude model for the emissivity of the striped wind and of the magnetic field within the dissipating stripes themselves. We calculate the polarization properties of the high-energy pulsed emission by generalising a method applied to gamma-ray burst models by Lyutikov et al. (2003), and discuss and compare our results with optical observations of the Crab pulsar.

2. Calculation of the Stokes Parameters

Our magnetic field model is based on the asymptotic solution of Bogovalov (1999), valid for $r \gg r_L$, and modified to take account of a finite width of the current sheet and with a small additional meridional component in the sheet, which serves to prevent the magnetic field from becoming identically zero. In order to simplify the Lorentz transformations, the small radial component of the field is neglected. In spherical polar coordinates (r, θ, φ) centered on the star and with axis along the rotation axis, the radial field is small ($B_r \sim B_L r_L^2/r^2$) and the other components are:

$$\begin{aligned} \{B_\theta, B_\varphi\} &= B_L \frac{r_L}{r} \{b_{1,2} \eta_\theta(\Delta_\theta, r, \theta, \varphi, t), \eta_\varphi(\Delta_\varphi, r, \theta, \varphi, t)\} \\ \eta_\varphi(\Delta_\varphi, r, \theta, \varphi, t) &= \tanh \left[\Delta_\varphi \left(\cos \theta \cos \alpha + \sin \theta \sin \alpha \cos \left\{ \varphi - \Omega_* \left(t - \frac{r}{v} \right) \right\} \right) \right] \\ \eta_\theta(\Delta_\theta, r, \theta, \varphi, t) &= \frac{1}{\Delta_\theta} \frac{\partial \eta_\varphi(\Delta_\theta, r, \theta, \varphi, t)}{\partial \varphi} \end{aligned} \quad (1)$$

Here, B_L is a fiducial magnetic field strength, v is the (radial) speed of the wind, $\Omega_* = c/r_L$ is the angular velocity of the pulsar, with r_L the radius of the light cylinder, α is the angle between the magnetic and rotation axes, $b_{1,2}$ are parameters controlling the magnitude of the meridional field in the two current sheets present in one wavelength, and $\Delta_{\theta,\varphi}$ are parameters quantifying the sheet thickness. The functional form of B_φ is motivated by exact equilibria of the planar relativistic current sheet (see Kirk & Skjæraasen 2003). However, in these equilibria the B_θ component, which has an important influence on the polarization sweeps, is arbitrary. The B_θ we adopt corresponds to a small circularly polarized component of the pulsar wind wave, such as is expected if the sheets are formed by the migration of particles within the wave, as described qualitatively by Michel (1971).

For the particle distribution, we adopt an isotropic electron/positron distribution given by $N(E, \vec{p}, \vec{r}, t) = K(\vec{r}, t) E^{-p}$ where $K(\vec{r}, t)$ is related to the number density of emitting particles. The radial motion of the wind imposes an overall $1/r^2$ dependence on this quantity, which is further modulated because the energization occurs primarily in the current sheet. The precise value in each sheet is chosen to fit the observed intensity of each sub-pulse. In addition, a small dc component is added, giving the off-pulse intensity. For the emissivity, we use the standard expressions for incoherent synchrotron radiation of ultrarelativistic particles in the Airy function approximation (Ginzburg & Syrovatskii 1969; Melrose 1971). Following Kirk et al. (2002), we assume the emission commences when the wind crosses the surface $r = r_0 \gg r_L$.

The calculation of the Stokes parameters as measured in the observer frame involves simply integrating the emissivity over the wind. However, this requires special care, because

the Lorentz boost from the rest frame of the emitting plasma involves not only beaming and Doppler shift, but also a change in the polarization angle due to the effects of aberration. Lyutikov et al. (2003) performed this calculation in the context of a gamma-ray burst model, assuming a relativistic shell of emitting plasma containing only a toroidal magnetic field. However, the relatively simple form of the emissivity function in that case means that two of the four Stokes parameters integrate to zero: $U = V = 0$, corresponding to linear polarization with constant position angle. Here we extend this method by adding a B_θ component and allowing for a more general, space and time dependent emissivity.

After straightforward but lengthy manipulations involving Lorentz transformations, we find the Stokes parameters as measured by an observer at time t_{obs} are given by the following integrals:

$$\left\{ \begin{array}{c} I_\omega \\ Q_\omega \\ U_\omega \end{array} \right\} (t_{\text{obs}}) = \int_{r_0}^{+\infty} \int_0^\pi \int_0^{2\pi} s_0(r, \theta, \varphi, t_{\text{ret}}) \left\{ \begin{array}{c} \frac{p+7/3}{p+1} \\ \cos(2\tilde{\chi}) \\ \sin(2\tilde{\chi}) \end{array} \right\} r^2 \sin\theta \, dr \, d\theta \, d\varphi \quad (2)$$

where the retarded time is given by $t_{\text{ret}} = t_{\text{obs}} + \vec{n} \cdot \vec{r}/c$ and \vec{n} is a unit vector along the line of sight from the pulsar to the observer. In this approximation the circular polarization vanishes: $V = 0$. The function s_0 is defined by:

$$s_0(r, \theta, \varphi, t) = \kappa K(\vec{r}, t) \omega^{-\frac{p-1}{2}} \mathcal{D}^{\frac{p+3}{2}} \left(\frac{B}{\Gamma} \sqrt{1 - (\mathcal{D} \vec{n} \cdot \vec{b})^2} \right)^{\frac{p+1}{2}} \quad (3)$$

where ω is the (angular) frequency of the emitted radiation, and κ is a constant factor that depends only on the nature of the radiating particles (charge q and mass m) and the power law index p of their distribution:

$$\kappa = \frac{\sqrt{3}}{2\pi} \frac{1}{4} \Gamma_{\text{Eu}} \left(\frac{3p+7}{12} \right) \Gamma_{\text{Eu}} \left(\frac{3p-1}{12} \right) \frac{|q|^3}{4\pi \varepsilon_0 m c} \left(\frac{3|q|}{m^3 c^4} \right)^{\frac{p-1}{2}} \quad (4)$$

with Γ_{Eu} the Euler gamma function and \mathcal{D} the Doppler boosting factor $\mathcal{D} = 1/\Gamma(1 - \vec{\beta} \cdot \vec{n})$. The direction of the local magnetic field in the observer's frame is given by the unit vector \vec{b} and the simplifying assumption has been made that this field has no component in the direction of the plasma velocity: $\vec{b} \cdot \vec{\beta} = 0$. (In this case the magnetic field transformation from the rest frame \vec{B}' to the observer frame \vec{B} is just $\vec{B}' = \vec{B}/\Gamma$ and, thus, its direction remains unchanged.) The angle $\tilde{\chi}$ measures the inclination of the *local* electric field with respect to the projection of the pulsar's rotation axis on the plane of the sky as seen in the observer's frame. The degree of linear polarization is defined by $\Pi = \sqrt{Q^2 + U^2}/I$. The corresponding polarization angle, defined as the position angle between the electric field vector at the observer and the projection of the pulsar's rotation axis on the plane of the sky is $\chi = 1/2 \arctan(U/Q)$.

3. Results

Using a model similar to that described above, Kirk et al. (2002) computed the total radiation intensity and compared the spacing of the resulting twin-pulse profile with observations of the Crab pulsar. They found an obliquity $\alpha = 60^\circ$ and an inclination of the rotation axis to the line of sight $\xi = \arccos(\vec{n} \cdot \vec{\Omega}_*/|\vec{\Omega}_*|) = 60^\circ$. In the following, we adopt these parameters, and set the radius at which emission switches on to be $r_0 = 30r_L$.

In the model of Kirk et al. (2002), the current sheet was assumed to be thin, which results in sharp profiles with very similar shapes for each of the subpulses. The upper left panel of Fig. 1 shows the intensity (Stokes parameter I) computed using our smoothed profile with $\Delta_\theta = 1$, $\Delta_\varphi = 5$, $b_1 = 0.1$ and $b_2 = 0.08$ for each subpulse. The electron density is $K = [\{(r_L B_L)/(r B)\}^{(p+1)/2} + \varepsilon - 1]/[r^2 (1 - 0.6 \eta_\theta)]$ where the parameter $\varepsilon = 0.05$ sets the minimum electron density between the current sheets (in normalized units). The denominator $(1 - 0.6 \eta_\theta)$ introduces an asymmetry in the relative pulse peak intensity. The variation of the magnetic field and the particle density along the line of sight, are shown in the bottom panels of Fig. 1.

The upper panels of Fig. 1 show the results of our computations on the left and the corresponding observed quantities (Kellner 2002; Kanbach et al. 2003) on the right. It should be noted that these data are preliminary. In particular, the measured degree of polarization may be subject to revision (Kanbach priv. comm.). Comparison with the upper right-hand panel shows that the model reproduces the observed pulse profile quite accurately. However, the idealised transverse geometry of the magnetic field in the (presumably turbulent) sheet leads to a rapid variation in phase of the term in parentheses on the right-hand side of Eq. (3), giving rise to a small notch-like feature visible in the peak of the sub-pulse, that proves difficult to eliminate. In this example, we adopted an electron power law index $p = 2$, as suggested by the relatively flat spectrum displayed by the pulsed emission between optical and gamma-ray frequencies (Shearer & Golden 2001; Kanbach 1998; Kuiper et al. 2001). Results are shown for two values of the Lorentz factor of the wind: $\Gamma = 20$ (solid line) and $\Gamma = 50$ (dotted line). For convenience, the maximum intensity is normalized to unity. The timescale is expressed in terms of pulse phase, 0 corresponding to the initial time $t = 0$ and 1 to a full revolution of the neutron star and thus one period $t = 2\pi/\Omega_*$.

The degree of polarization is shown in the two middle panels of Fig. 1. According to our computations (left-hand panel) this displays a steady rise in the initial off-pulse phase, that steepens rapidly as the first pulse arrives. During the pulse phase itself, the polarization shrinks down to about 10%. Theoretically the maximum possible degree of polarization is closely related to the index p of the particle spectrum. In the most favorable case of a uniform magnetic field, it is given by $\Pi_{\max} = (p + 1)/(p + 7/3)$.

However, in the curved magnetic field lines of the wind, contributions of electrons from different regions have different polarization angles. Consequently, they depolarize the overall result when superposed. We therefore expect a degree of polarization that is at most Π_{\max} . For the example shown in figure 1, $\Pi_{\max}(p = 2) = 69.2\%$, well above the computed value, which peaks at 52%.

The lower panels of Fig. 1 show the polarization angle, measured against celestial North and increasing from North to East. Our model predicts this angle relative to the projection of the rotation axis of the neutron star on the sky, which we take to lie at a position angle of 124° , following the analysis of Ng & Romani (2004). In the off-pulse stage, the electric vector of our model predictions lies almost exactly in this direction, since it is fixed by the orientation of the dominant toroidal component B_φ of the magnetic field. Such a relation between the off-pulse angle of polarization and the toroidal magnetic field at large distance (**close to** the light cylinder) was already suggested by Smith et al. (1988). In the rising phase of the first pulse, B_φ decreases, whereas B_θ increases, causing the polarization angle to rotate from its off pulse value by about 50° , for the chosen parameters. However, for a weaker B_θ contribution, as in the second pulse, the swing decreases. This effect can also be caused by a relatively large beaming angle, (i.e., low Lorentz factor wind). The basic reason is that contributions from particles well away from the sheet center are then mixed into the pulse, partially canceling the contribution of the particles in the center of the current sheet, which favor $\chi = 124^\circ \pm 90^\circ$, and enforcing $\chi = 124^\circ$. On the other hand, a very high value of the Lorentz factor or large values of $b_{1,2}$ reduce the off-center contribution, leading, ultimately, to the maximum possible 90° sweep between off-pulse (B_φ -dominated) and center-pulse (B_θ -dominated) polarizations, followed by another 90° sweep in the same sense when returning to the off-pulse. Thus, in general, in the middle of each pulse, the polarization angle is either nearly parallel to the projection of the rotation axis, or nearly perpendicular to it, depending on the strength of B_θ and on Γ . This interpretation is confirmed by computations with $\Gamma = 50$ that show a larger sweep, as shown in Fig. 1.

The optical polarization measurements suggest that in the centre of the pulses the position angle is close to 124° . In the declining phase of both pulses, the angle reaches a maximum before returning to the off-pulse orientation. Note that in both cases the swing starts in the same direction, (counterclockwise in figure 1). This is determined by the rotational behavior of the B_θ component, implying that this changes sign between adjacent sheets, as in Eq. (1). The observed off-pulse position angle is closely aligned with the projection of the rotation axis of the pulsar, in accordance with the model predictions.

In addition to models aimed at providing a framework for the interpretation of the emission of the Crab pulsar, we have performed several calculations with different Lorentz

factors Γ , injection spectrum of relativistic electrons p and inclinations of the line of sight ξ . The general characteristics of the results are: For low Lorentz factors, independent of p and ξ , the relativistic beaming becomes weaker and the pulsed emission is less pronounced, because the observer receives radiation from almost the entire wind. For instance, taking $\Gamma = 2$ and $p = 2$ or 3 , the average degree of polarization does not exceed 20 % and the swing in the polarization angle is less than 30° . For high Lorentz factors $\Gamma \geq 50$, the strong beaming effect means that the observer sees only a small conical fraction of the wind. The width of the pulses is then closely related to the thickness of the transition layer. The degree of linear polarization flattens in the off-pulse emission while it shows a sharp increase followed by a steep decrease during the pulses. Due to the very strong beaming effect, only a tiny part of the wind directed along the line of sight will radiate towards the observer. In the off-pulse phase, the polarization angle is then dictated solely by the B_φ component “attached” to the line of sight, and the degree of linear polarization remains almost constant in time. For very high Lorentz factors, the behavior of polarization angle and degree remain similar to those of Fig. 1, with perfect alignment between polarization direction (electric vector) and the projection of the pulsar’s rotation axis on the plane of the sky in the off-pulse phase and two consecutive polarization angle sweeps of 90° in the same sense during the off-pulse to center-pulse and center-pulse to off-pulse transitions. This mirrors the fact that emission comes only from a narrow cone about the line of sight of half opening angle $\theta \approx 1/\Gamma$.

For given values of Γ and ξ , the particle spectral index p affects only the average degree of polarization degree but not the light curve nor the polarization angle. For example, taking $\Gamma = 10$ and $\xi = 60^\circ$, a spectral index of $p = 2$ leads to an average polarization of $\tilde{\Pi} = 19.2\%$ whereas for $p = 3$ it leads to $\tilde{\Pi} = 30.8\%$.

4. Conclusions

In the striped wind model, the high energy (infra-red to gamma-ray) emission of pulsars arises from outside the light cylinder, in accordance with the early suggestions of Pacini & Rees (1970) and Shklovsky (1970). It provides an alternative to the more intensively studied polar cap, outer gap and two-pole caustic models. All models contain essentially arbitrary assumptions concerning the configuration of the emission region and the distribution function of the emitting particles, rendering it difficult to distinguish between them on the basis of observations. However, the geometry of the magnetic field, which is the crucial factor determining the polarization properties, is constrained in the striped model to be close to that of the analytic asymptotic solution presented by Bogovalov (1999). We have therefore presented detailed computations of the polarization properties of the pulses expected in

this scenario. These possess the characteristic property, unique amongst currently discussed models, that the electric vector of the off-pulse emission is aligned with the projection of the pulsar’s rotation axis on the plane of the sky. This is in striking agreement with recent observations of the Crab pulsar. In addition the striped wind scenario naturally incorporates features of the phase-dependent properties of the polarization angle, degree of polarization and intensity that are also seen in the data. This underlines the need to develop the model further, in order to confront high-energy observations of the Crab and other pulsars. In particular, the manner in which magnetic energy is released into particles in the current sheet remains poorly understood and the link between the asymptotic magnetic field structure and the pulsar magnetosphere is obscure.

We thank Gottfried Kanbach for providing us with the OPTIMA data and for helpful discussions. This work was supported by a grant from the G.I.F., the German-Israeli Foundation for Scientific Research and Development.

REFERENCES

- Bogovalov, S. V. 1999, *A&A*, 349, 1017
- . 2001, *A&A*, 371, 1155
- Cheng, K. S., Ho, C., & Ruderman, M. 1986, *ApJ*, 300, 500
- Coroniti, F. V. 1990, *ApJ*, 349, 538
- Dyks, J., Harding, A. K., & Rudak, B. 2004, *ApJ*, 606, 1125
- Dyks, J., & Rudak, B. 2003, *ApJ*, 598, 1201
- Ginzburg, V. L., & Syrovatskii, S. I. 1969, *ARA&A*, 7, 375
- Harding, A. K. 2001, in *American Institute of Physics Conference Series #558*, 115
- Hirovani, K., & Shibata, S. 1999, *MNRAS*, 308, 54
- Kanbach, G. 1998, *Advances in Space Research*, 21, 227
- Kanbach, G., Kellner, S., Schrey, F. Z., Steinle, H., Straubmeier, C., & Spruit, H. C. 2003, in *Instrument Design and Performance for Optical/Infrared Ground-based Telescopes*. Edited by Iye, Masanori; Moorwood, Alan F. M. *Proceedings of the SPIE*, Volume 4841, pp. 82-93 (2003)., 82–93

- Kellner, S. 2002, Master’s thesis, Technische Universität München
- Kirk, J. G., & Skjæraasen, O. 2003, *ApJ*, 591, 366
- Kirk, J. G., Skjæraasen, O., & Gallant, Y. A. 2002, *A&A*, 388, L29
- Kuiper, L., Hermsen, W., Cusumano, G., Diehl, R., Schönfelder, V., Strong, A., Bennett, K., & McConnell, M. L. 2001, *A&A*, 378, 918
- Lyubarskii, Y. E. 1996, *A&A*, 311, 172
- Lyubarsky, Y., & Kirk, J. G. 2001, *ApJ*, 547, 437
- Lyutikov, M., Pariev, V. I., & Blandford, R. D. 2003, *ApJ*, 597, 998
- Melrose, D. B. 1971, *Ap&SS*, 12, 172
- Michel, F. C. 1971, *Comments on Astrophysics and Space Physics*, 3, 80
- . 1994, *ApJ*, 431, 397
- Ng, C.-Y., & Romani, R. W. 2004, *ApJ*, 601, 479
- Pétri, J., Heyvaerts, J., & Bonazzola, S. 2002, *A&A*, 384, 414
- Pacini, F., & Rees, M. J. 1970, *Nature*, 226, 622
- Romani, R. W., & Yadigaroglu, I.-A. 1995, *ApJ*, 438, 314
- Ruderman, M. A., & Sutherland, P. G. 1975, *ApJ*, 196, 51
- Shearer, A., & Golden, A. 2001, *ApJ*, 547, 967
- Shklovsky, I. S. 1970, *ApJ*, 159, L77
- Smith, F. G., Jones, D. H. P., Dick, J. S. B., & Pike, C. D. 1988, *MNRAS*, 233, 305
- Sturrock, P. A. 1971, *ApJ*, 164, 529
- Vlahakis, N. 2004, *ApJ*, 600, 324

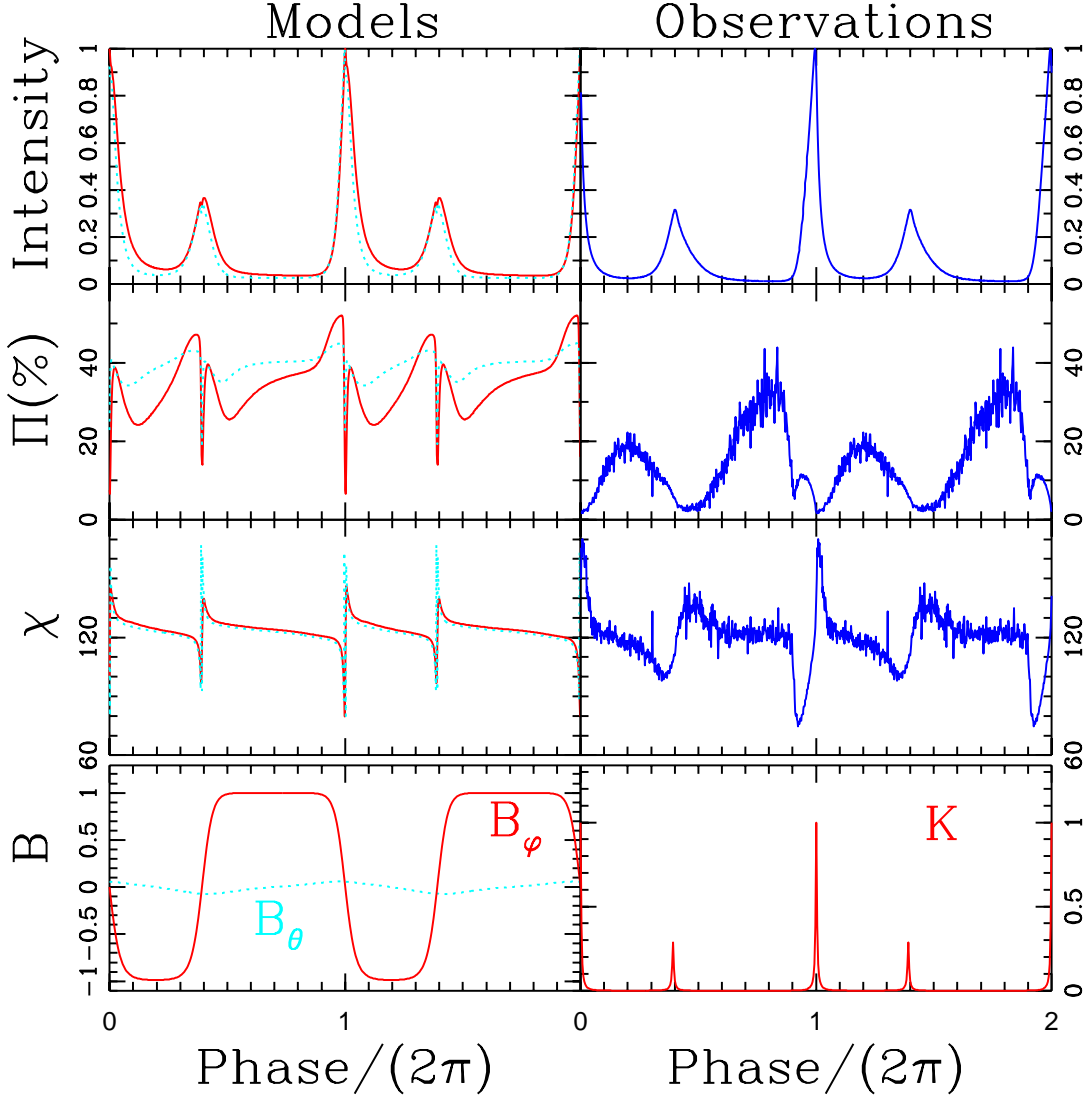


Fig. 1.— Light curve of intensity, degree of polarization and position angle of the pulsed synchrotron emission obtained by numerical integration of the set of equations (2), and measurements of these quantities for the Crab pulsar (Kellner 2002; Kanbach et al. 2003). Models with Lorentz factor $\Gamma = 20$ (solid line, red online) and 50 (dotted line, cyan online) are shown. The assumed particle energy distribution index was $p = 2$, and the inclination of the line of sight equals the obliquity: $\alpha = \xi = 60^\circ$. The position angle of the projection of the pulsar’s rotation axis was set to 124° (Ng & Romani 2004). The bottom panels show the dependence on phase ($= \Omega_* r / (2\pi v)$ in Eq. (1)) of the assumed magnetic field components and the particle density in the comoving frame. The maximum values of B_φ and K are normalized to unity.